Geochemistry Geophysics Geosystems G3

*Technical Brief*
Volume 14, Number 10
7 October 2013
doi: 10.1002/ggge.20225
ISSN: 1525-2027

Published by AGU and the Geochemical Society

# Millimeter-level precision in a seafloor geodesy experiment at the Discovery transform fault, East Pacific Rise

**Jeffrey J. McGuire and John A. Collins**

*Department of Geology and Geophysics, Woods Hole Oceanographic Institution, Woods Hole, Massachusetts, 02543, USA (jmcguire@whoi.edu)*

[1] Direct-path acoustic ranging is a promising seafloor geodetic technique for continuous high-resolution monitoring of geodynamical process such as fault slip and magma intrusion. Here we report on a yearlong acoustic ranging experiment conducted across the discovery transform fault at ~4°S on the East Pacific Rise. The ranging instruments utilized a novel acoustic signal designed to enhance precision. We find that, after correcting for variations in sound speed at the path end-points, the ranging measurements have a precision of ~1 mm over baselines approaching 1 km in length. The primary difficulty in this particular experiment was with the physical stability of the benchmarks, which were deployed free fall from a ship. Despite the stability issues, it appears that the portion of the transform fault that the array covered was locked during the year of our survey. The primary obstacle to continuous, high sample rate, high-precision geodetic monitoring of oceanic ridges and transform faults is now limited to the construction of geodetic monuments that are well anchored into bedrock.

**Components:** 4,736 words, 11 figures.

**Keywords:** seafloor geodesy; oceanic transform fault.

**Index Terms:** 1294 Instruments and techniques: Geodesy and Gravity; 1242 Seismic cycle related deformations: Geodesy and Gravity; 6924 Interferometry: Radio Science; 7209 Earthquake dynamics: Seismology; 7223 Earthquake interaction, forecasting, and prediction: Seismology; 7230 Seismicity and tectonics: Seismology; 8118 Dynamics and mechanics of faulting: Tectonophysics; 8004 Dynamics and mechanics of faulting: Structural Geology.

**Received** 20 May 2013; **Revised** 12 July 2013; **Accepted** 12 July 2013; **Published** 7 October 2013.

McGuire, J. J., and J. A. Collins (2013), Millimeter-level precision in a seafloor geodesy experiment at the discovery transform fault, East Pacific Rise, *Geochem. Geophys. Geosyst.*, *14*, 4392–4402, doi:10.1002/ggge.20225

## 1. Introduction

[2] More than 75% of the deformation taken up by fault slip at both spreading centers and transform faults on the Earth's mid-ocean ridge system occurs aseismically without earthquakes [*Bird et al*., 2002; *Boettcher and Jordan*, 2004; *Cowie et al*., 1993]. Despite being the dominant deformation mechanism within the lithosphere along the Earth's mid-ocean ridge system, this aseismic fault creep has not yet been directly observed owing to the technological difficulties involved in making geodetic measurements on the seafloor. Instead, aseismic fault creep is inferred from seismic moment budgets, plate-motion velocities, and earthquake catalogs. While some continental strike-slip faults creep continuously others fail in transient creep events with durations of hours to days that typically have surface offsets of a few millimeters to a few centimeters. Observing the details of how the creep occurs on mid-ocean ridge faults would enable us to differentiate between

different models of fault frictional properties as has been done for continental systems [*Wei et al*., 2013]. Additionally, better constraints on fault rheology, particularly the role of serpentine in enabling shallow creep, would improve our understanding of the strength of oceanic plate boundaries.

[3] Transient creep events have been inferred to control the timing of large earthquakes on many oceanic transform faults, owing to the properties of earthquake swarms that are routinely observed on these faults [*McGuire et al*., 2005, 2012; *Roland and McGuire*, 2009]. In contrast to the predominantly aseismic slip, there are short segments of oceanic transform faults that appear to be fully coupled and fail in repeating large earthquakes that rerupture the same asperity quasiperiodically, often during earthquake swarms [*Boettcher and McGuire*, 2009; *McGuire*, 2008]. Improving our understanding of the partitioning of plate motion between seismic and aseismic slip, as well as the role of transient creep events in earthquake triggering, will require the development of high precision, continuous seafloor geodetic measurements to map out the space-time relationships between creep events and large earthquakes.

[4] Many of the most successful approaches to seafloor geodesy undertaken to date have relied on precise timing of acoustic signals transmitted between two or more instruments. These experiments obtain either relative strain (e.g., baseline length changes) between two seafloor-based sensors [*Chadwick et al*., 1999] or absolute position measurements in the GPS reference frame if one of the acoustic sensors is mounted on a surface ship or buoy [*Gagnon et al*., 2005]. Ship/surface-based measurements have the advantage of being placed in the global reference frame, whereas relative seafloor-based measurements typically have higher precision because their acoustic paths do not pass through the mixed layer at the sea surface where the sound velocity is highly temporally and spatially variable. Seafloor-based measurements of strain are also easier to obtain continuously at a high sample rate. The primary limitations on their accuracy result from the stability of the seafloor benchmark, the accuracy of corrections for sound speed variations, and the precision of the acoustic travel time measurement. Rather than attempting to synchronize clocks between two distant sensors, most ranging experiments measure the two-way (round-trip) travel time between two sensors where one acts as a "mirror transponder" that retransmits the received acoustic signal following a fixed delay [*Spiess et al*., 1998]. The round-trip travel time can be measured with an accuracy that depends on the signal design, but is typically equivalent to 1 cm or better (i.e., O $\sim$10 μs). For baselines on the scale of a few hundred meters, the dominant error source is typically the variation in sound speed, often of the order of tens of cm (O $\sim$100 μs) for paths of a few hundred meters, which must be accounted for by using independent measurements of temperature, salinity, and pressure [*Chadwick et al*., 1999].

[5] An early successful experiment by *Chadwick et al*. [1999] used short bursts (five cycles) of a 50 kHz signal to measure 100–400 m baselines with a precision of $\sim$1 cm. This precision was sufficient to record signals of a few cm in amplitude from both the slow inflation and the rapid eruption of the magma chamber beneath axial seamount on the Juan de Fuca ridge [*Chadwick et al*., 1999]. Similar instruments were able to demonstrate that spreading on the cleft segment of the Juan De Fuca ridge must be episodic and not continuous [*Chadwell and Spiess*, 2008; *Chadwell et al*., 1999; *Chadwick and Stapp*, 2002]. More recently, a similar experiment by *Osada et al*. [2012] using a 10 kHz coded signal [*Osada et al*., 2008] achieved $\sim\pm$1.5 cm scatter over a baseline of $\sim$900m. They attributed much of the residual scatter to inaccuracies in the corrections for sound speed variations. A recent technique innovation by *Blum et al*. [2010] is to suspend one of the acoustic transponders in the water column 5–10 m above the seafloor. While this introduces a new source of error (the motion of the suspended transponder in the current), it has great promise for allowing ranging to cover significant baselines in regions of rough and/or sloping seafloor where direct paths are difficult to obtain using only seafloor-based benchmarks which are typically $\leq$3m tall. Blum et al. obtained a $\pm$2.5 cm accuracy for 1000 m baselines, which when averaged over 20 interrogations, yielded uncertainties of about 6 mm in daily baseline length measurements [*Blum et al*., 2010].

[6] In 2008, we conducted a yearlong deployment of an acoustic ranging system at the Discovery transform fault at $\sim$4°S on the equatorial East Pacific Rise (EPR) (Figure 1). The geodetic array was part of a larger scale deployment of ocean bottom seismographs aimed at studying the seismicity of the Quebrada-Discovery-Gofar (QDG) transform fault system [*McGuire et al*., 2012]. The QDG system exhibits a range of frictional behavior including fully coupled patches on the Gofar and Discovery transform faults that rupture

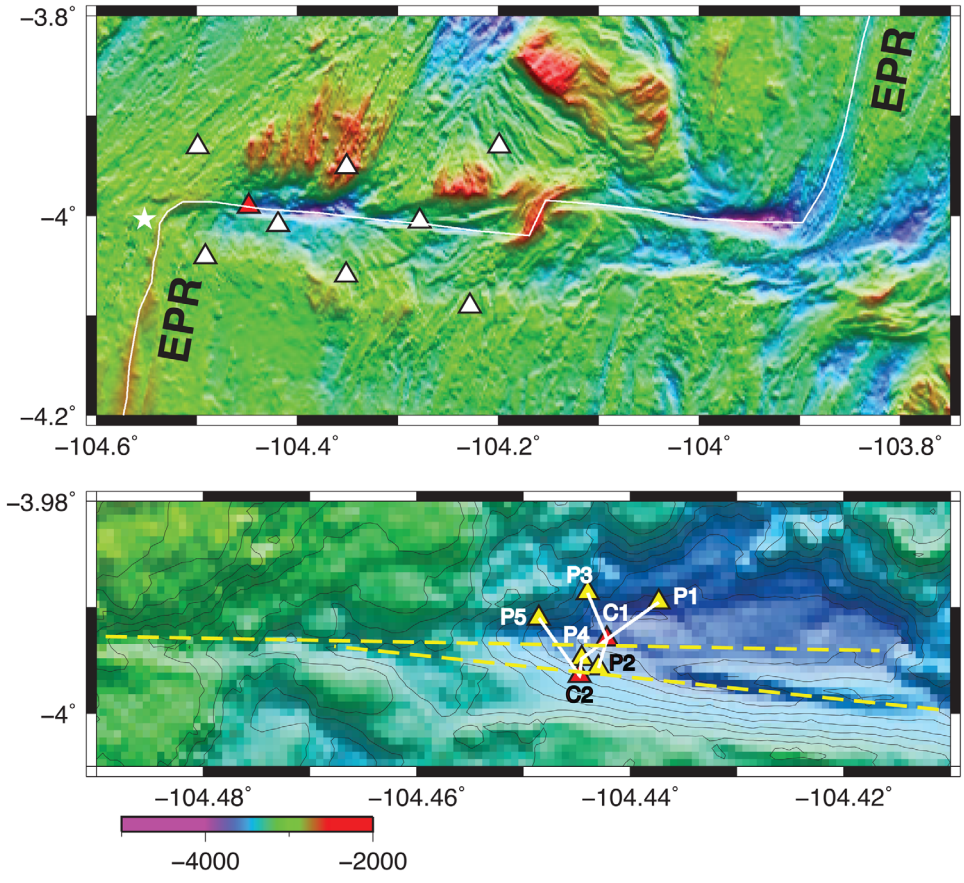


**Figure 1.** Map of the Discovery transform experiment. (top) the large-scale geologic structure of the region with bathymetry and plate-boundary locations (white line) from *Pickle et al*. [2009]. White triangles denote the locations of ocean bottom seismographs. A star denotes the approximate location of a pair of M4.2 earthquakes on 6/19/2008 which were the largest events recorded by the seismometer array. The red triangle shows the location of the acoustic ranging array. (bottom) Zoom-in of the region of the acoustic ranging experiment with detailed EM300 multibeam bathymetry [*Wolfson et al*., 2011]. Triangles and labels show the location of acoustic transceivers (red) and transponders (yellow). The dashed yellow lines denote possible surface traces of the plate boundary fault system based on the locations of valleys in the bathymetry.

repeatedly in M∼6 earthquakes, as well as the nearly aseismic Quebrada fault that has experienced only one earthquake larger than M5.5 since 1990 [*McGuire*, 2008]. The instruments consisted of a tripod base with the acoustic transducer located at the top of a mast secured with guide wires for stability (Figure 2). The array was deployed by free fall from a ship. Owing to the difficulty in positioning the instruments via free fall and the rough topography, several were repositioned during the deployment cruise to maximize the number of acoustic baselines and increase the likelihood that the baselines crossed the primary transform fault strand inferred from multibeam bathymetry and acoustic backscatter data [*Pickle et al*., 2009; *Wolfson et al*., 2011]. The exact trace of the plate boundary has not been mapped via submersible or remotely operated vehicle (ROV), but based on the alignment of the main fault valleys in the EM300 bathymetry, it is very likely that the surface trace of the fault is spanned by multiple baselines within our array (Figure 1). The purpose of this paper is to present the precision of the acoustic ranging measurements, their implications for the locking state of the fault in this region, and to provide suggestions for future acoustic ranging experiments.

## 2. Data

[7] We deployed seven acoustic ranging tripods across the expected trace of the Discovery transform fault in December 2007 and recovered them in January 2009. The tripods were ∼3 m tall (Figure 2) with the acoustic transducer located atop a

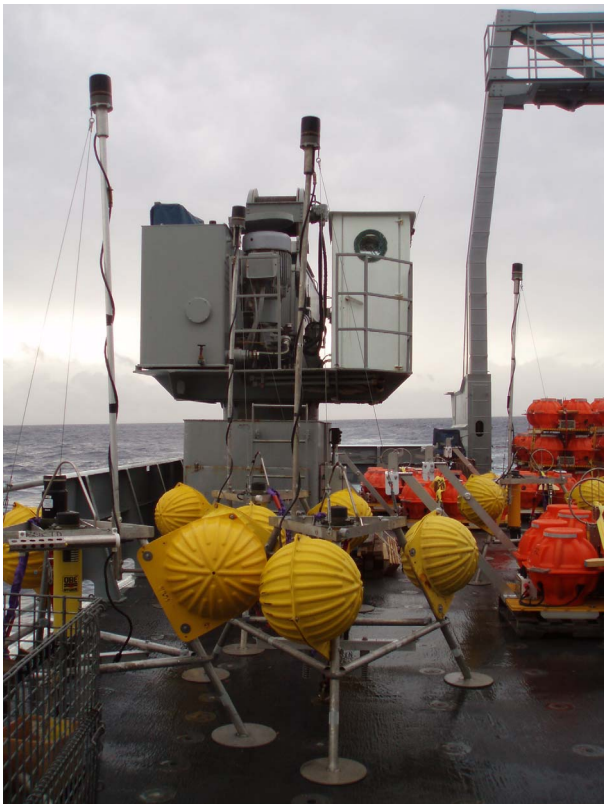

**Figure 2.** Acoustic ranging tripods on the deck of the R/V Thomas G. Thompson, December 2007.

mast that was secured with guide wires to limit mechanical vibrations of the mast (Figure 2). The tripods were of two types: two master transceivers that interrogated five mirror transponders. The transceivers are labeled C1 and C2 in Figure 1, while the transponders are labeled P1, P2, P3, P4, and P5. We recorded a full years worth of data on the C1-P1, C1-P2, C1-P3, and C2-P5 baselines. Transponder P4's glass ball, which housed the electronics, appears to have flooded in March 2008 ending data acquisition on the C1-P4 and C2-P4 baselines. The transceivers were equipped with acoustic modems so the data could be accessed from the ship. Several of the instruments had to be repositioned after their initial deployments owing to a lack of acoustic line of sight between instruments. However, depending on the exact trace of the fault, it is likely that the C2-P5 and possibly also the C1-P2 baselines cross the fault trace (Figure 1). Each tripod was equipped with a conductivity-temperature sensor for monitoring changes in sound speed.

[8] The acoustic systems were manufactured by Linkquest Technologies Inc. (http://www.linkquest.com). Each mirror transponder was interrogated every 2 h by one or both transceivers. The instruments utilize a 10 kHz signal that is comprised of a 512 bit pseudorandom code (four cycles per bit). The code is designed such that the correlation of the outgoing and incoming signals yields as close to a unique peak as possible. For each measurement, either the full raw pressure waveform at the transceiver sampled at 16 samples/cycle (e.g., 16 × 10 kHz) or just the correlation function (to save disk space on most measurements) was recorded. Figure 3 shows an example of the raw pressure waveform recorded by C1 for the C1-P1 baseline and the resulting correlation function (only 512 samples surrounding the maximum are typically saved). The round-trip travel times are measured from the peak of the correlation function computed by a simple quadratic interpolation to the three contiguous samples that include the correlation maximum. The top plot in Figure 4 shows these measurements of the round-trip travel time, which we term the raw measurements, plotted as distance assuming a nominal 1500 m/s sound speed. The raw measurements are dominated by a long-term annual variation with amplitude of about 20 cm. There is also a clear "cycle skipping" problem beginning around time 2008.5 where the maximum of the correlation function oscillates between two adjacent peaks resulting in two parallel curves. The middle plot of Figure 4 shows the two nearly identical temperature records recorded at C1 and P1. The variation in the temperature record is effectively the inverse of the variation in the ranges in the top plot, demonstrating that the major source of error in the top plot results

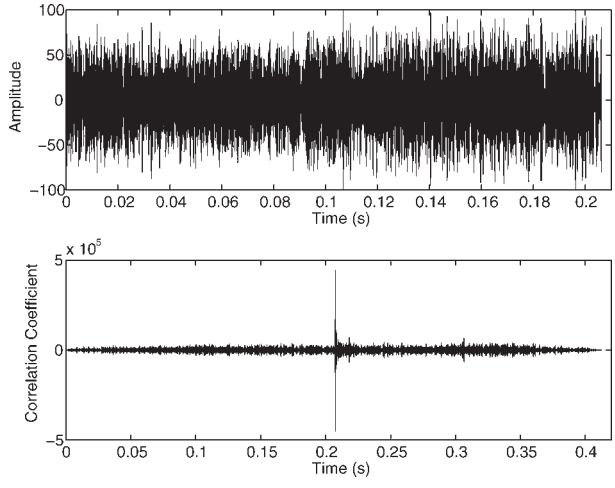


**Figure 3.** An example of (top) a raw waveform and (bottom) a correlation function for that waveform from the C1-P1 baseline.

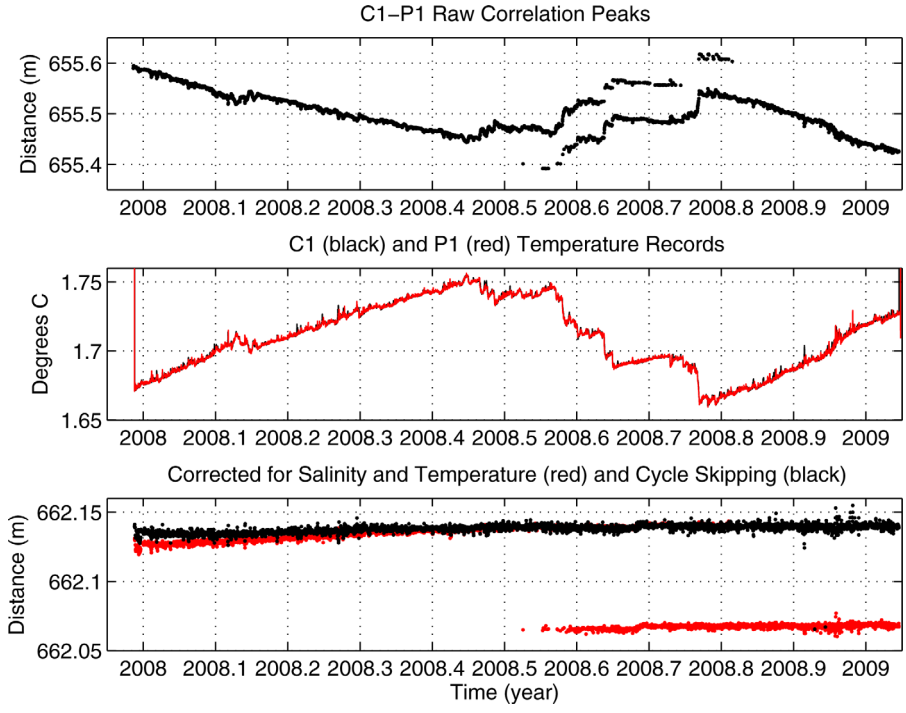


**Figure 4.** Ranges for C1-P1. (top) The raw peaks of the correlation function. Cycle skipping is visible from times 2008.5 through 2008.8. (middle) The temperature variations recorded at C1 and P1 are nearly identical. (bottom) The raw correlation peaks corrected for the variations in sound speed inferred from measurements of salinity and temperature (shown in red). These corrections do not account for the cycle skipping problem. The black dots show the travel-time measurements derived by cross correlating the correlation functions. This approach fixes the cycle skipping issue.

from temporal changes in sound speed. Correcting the raw measurements for the sound-speed variations resulting from the salinity and temperature changes results in the red points plotted in the bottom plot of Figure 4. This correction removes the vast majority of the variation in the raw measurements except for the cycle skipping problem.

[9] We use two approaches to address the cycle skipping problem. The top plot of Figure 5 shows an example of the cycle skipping artifact. The blue and red correlation functions are taken 2 h apart on the C1-P1 baseline and are nearly identical, indicating that there was little change in the baseline length over these 2 h. However, owing to complications with the acoustic propagation path, such as from bottom interaction and/or multipathing, the peak of the correlation function is not sharp and the numerical maximum oscillates between two cycles as shown by the red and blue crosses that denote the maximum values in these particular measurements. This one-cycle ambiguity corresponds to about 7.3 cm in range. In some cases, the easiest fix to this ambiguity is simply to pick the (better defined) minimum rather than the maximum of the correlation function for a particular baseline. However, this often does not solve the problem for all measurements. The second approach is to cross-correlate the correlation functions from two measurements to determine the change in travel time between them. The middle and bottom plots of Figure 4 illustrate this approach. The blue and red correlation functions from the top plot have been cross-correlated with a reference correlation function shown in black. Both result in minimal time shifts ($\sim$10 ms $\approx$6 mm) relative to the black trace. Thus, despite the difference in their raw peaks, by correlating the correlation functions, we are able to correctly identify that the blue and red correlation functions record nearly identical travel times. The black dots in the bottom plot of Figure 4 show the entire year of C1-P1 ranges corrected for the cycle skipping in this way, in addition to the corrections for sound speed variations. The remaining variation over the year is very small ($<$1 cm). The choice of the reference correlation function is determined by trial and error, but any clean, high signal-to-noise ratio (SNR) measurements with a well-defined main peak usually works.

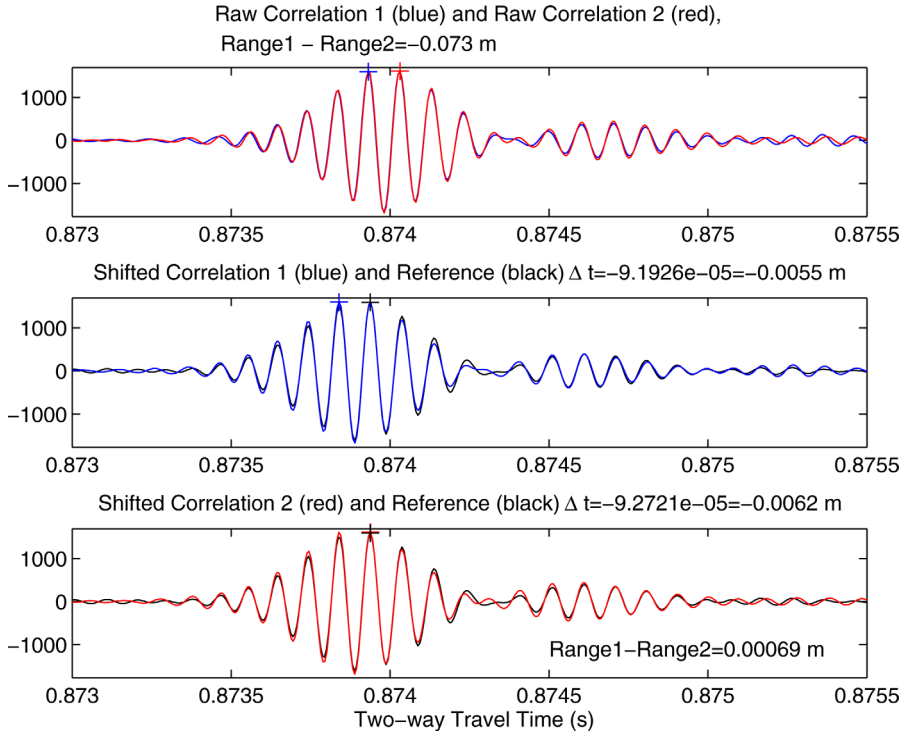


**Figure 5.** (top) Two cross correlation functions from measurements on the C1-P1 baseline taken 2 h apart. They are nearly identical, but due to small differences in their shape, their maximum values (denoted by the plus marks) occur on adjacent cycles. If this difference were interpreted as a true travel time difference it would amount to a 7.3 cm discontinuity in the range time series. (middle) The first correlation function (blue) has been cross-correlated with a reference waveform (black), finding an offset of ∼6 mm which results primarily from sound speed changes. (bottom) Similar to the middle plot but for the red correlation function. The agreement in the offsets (5.5 versus 6.2 mm) between the middle and bottom plots demonstrates that this approach does not have the cycle skipping problem.

## 3. Results

[10] The bottom plots of Figures 4 and 6–8 present the time series of ranges corrected for both sound speed variations and cycle skipping for the four baselines with a year's worth of data. In all four cases, the cycle-skipping correction works for the majority of affected measurements but there are still a few uncorrected measurements. The C1-P1, C1-P2, and C1-P3 time series all show remarkably stable ranges with very little variation with the exception of a −4 cm step on 19 June 2008 in the C1-P3 baseline. This step coincides with a pair of $M_w$ 4.2 strike-slip earthquakes that were located about 10 km to the west of the array on the transform fault near the ridge-transform intersection (Figure 1). Given the distance from the array to the earthquakes, this offset is unlikely due to slip on a fault crossing the C1-P3 baseline and is more likely due to instability of the benchmark.

[11] The C2-P5 time series is more complicated with a general trend toward increasing ranges at a rate of ∼3 cm/yr combined with a number of steps including a −2 cm offset on 19 June similar to that seen in the C1-P3 time series. Each instrument was equipped with a tilt sensor to measure monument instability. Unfortunately, most of these sensors returned poor quality data. However, one exception is the tilt data recorded on P3 which shows its only change as a ∼1.5° step on 19 June (Figure 9), confirming the hypothesis that the step offsets in the C1-P3 and C2-P5 time series likely result from instrument instability rather than fault motion. The instability of the benchmarks is not surprising given that they were deployed by free fall from a ship in water depths of over 2500 m into a region of very steep terrain and rough seafloor. Future deployments could likely overcome this issue through ROV-based benchmark installations.

[12] Despite the benchmark instabilities, the corrected time series in Figures 4–8 demonstrate that the ability of the acoustic processing to measure relative distance changes is extremely precise.

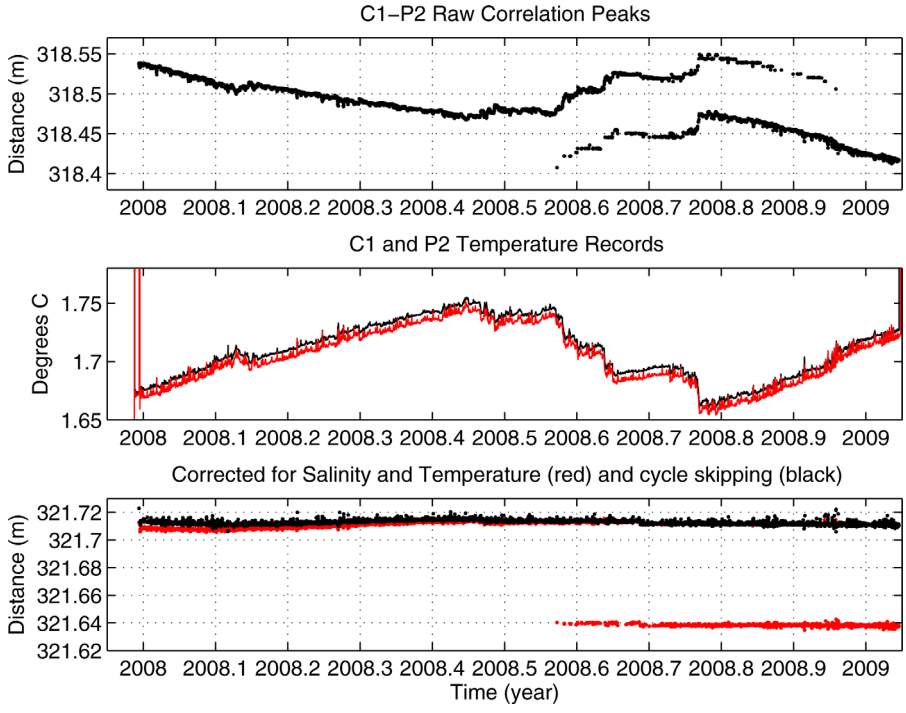


**Figure 6.** C1-P2 ranges, temperatures, and corrected ranges similar to Figure 4.

Figure 10 shows histograms of corrected ranges from each of the four baselines. Each histogram covers an approximately 2 month time period when there were no visible offsets in the time series. The standard deviations of the individual measurements range from 1.2 to 2.0 mm for the various baselines. The largest scatter, 2.0 mm, is for the C2-P5 baseline. However, part of this

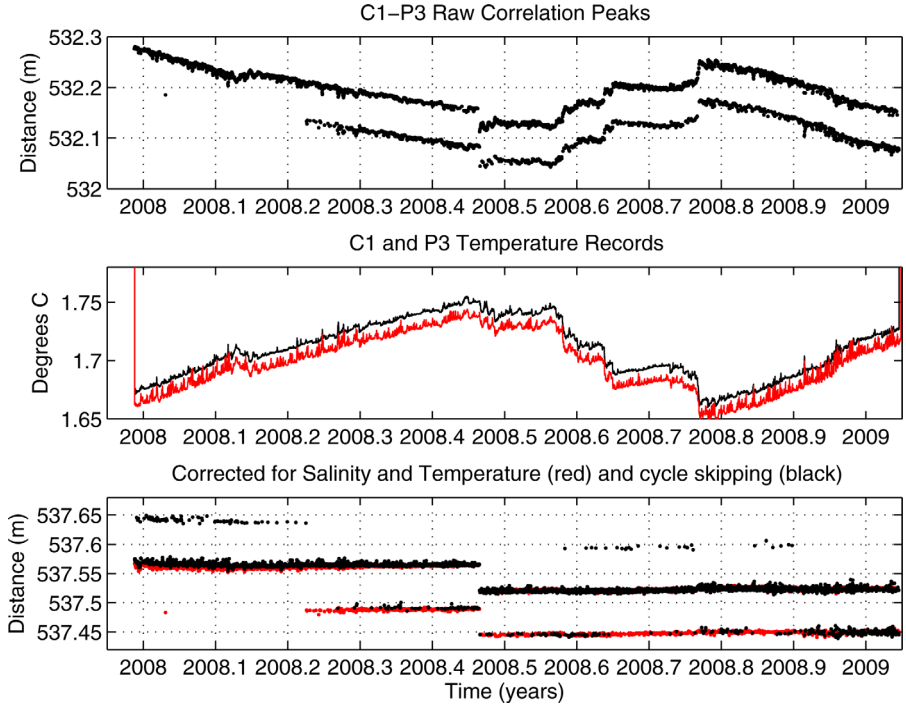


**Figure 7.** Ranges, temperatures, and corrected ranges for the C1-P3 baseline similar to Figure 4.

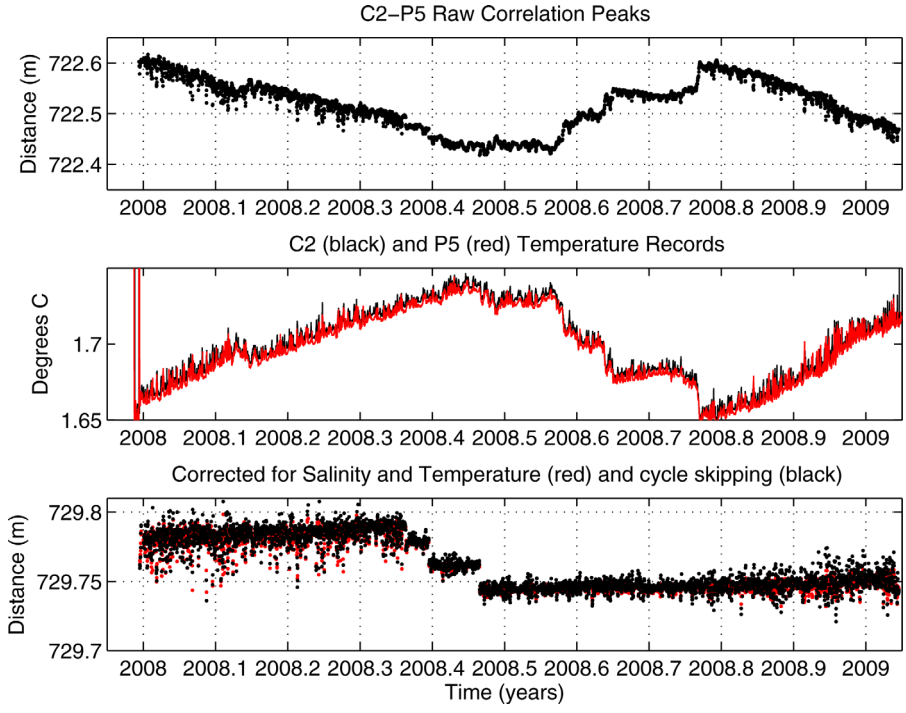


**Figure 8.** Ranges, temperatures, and corrected ranges for the C2-P5 baseline.

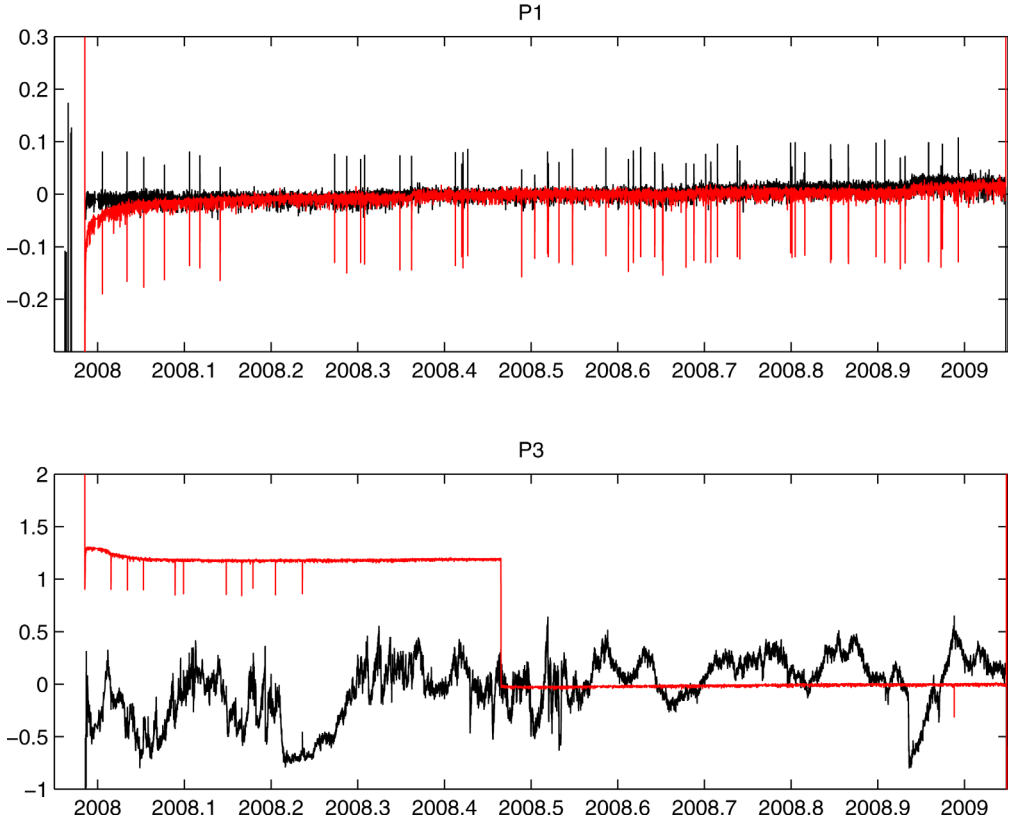


**Figure 9.** The red and black curves denote the two orthogonal components of tilt recorded within the instrument sensor balls on the P1 and P3 tripods. The unusually large variations in the black component of P3 may indicate that this component was not functioning properly.

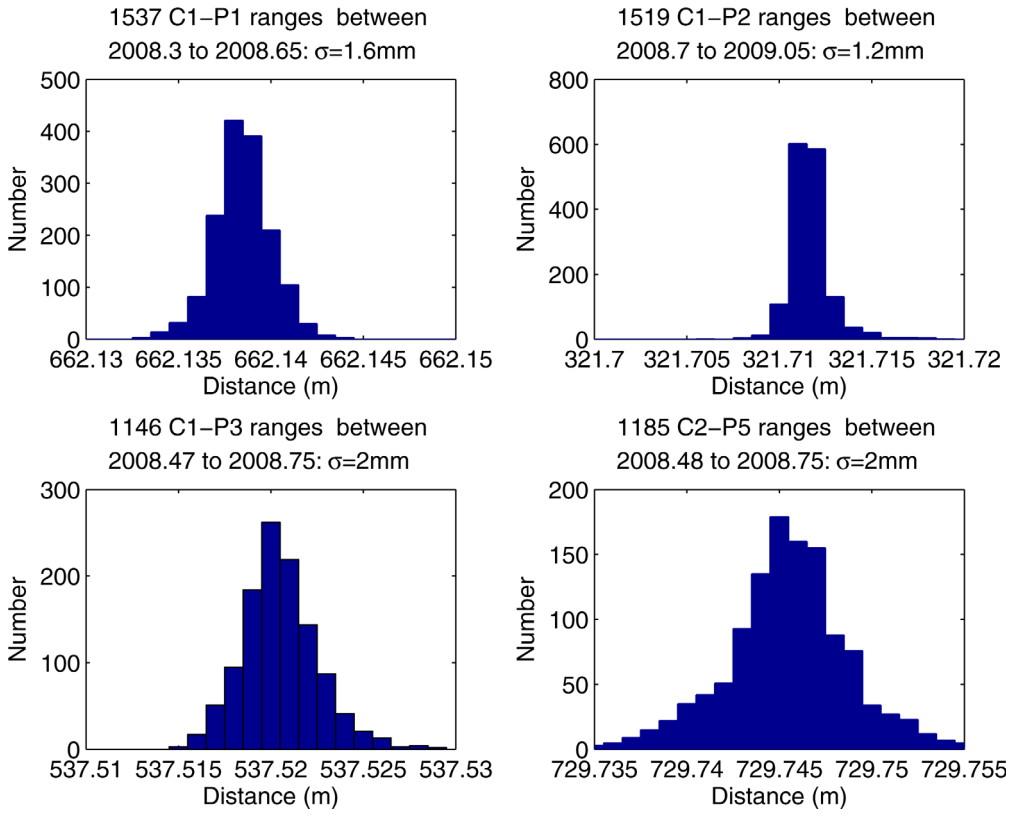


**Figure 10.** Histograms of range measurements that have been corrected for cycle skipping. Each histogram shows all ranges for a ∼2–4 month period when there were no offsets in the time series for that baseline. All histograms span 2 cm in range along the horizontal axis for ease of comparison. Standard deviations of the measurements for different baselines range from 1.2 to 2.0 mm and likely reflect the complexity of multipathing for each path. The C2-P5 histogram is likely affected by the overall trend toward increasing range with time seen in this baseline.

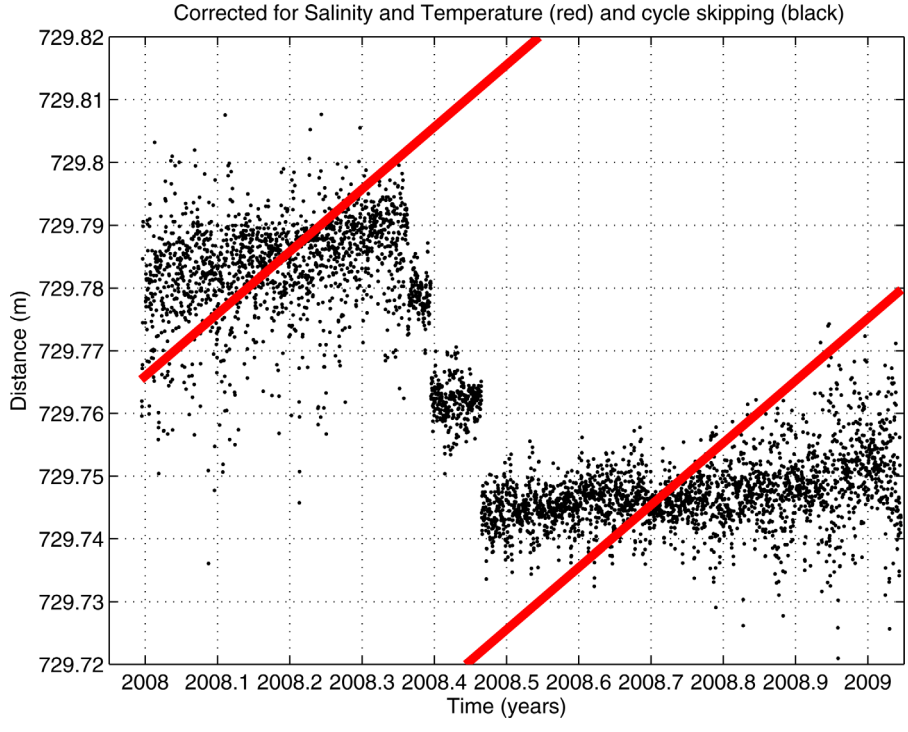


**Figure 11.** Ranges for the C2-P5 baseline. The time series shows a general trend toward increasing ranges at a rate of 1–2 cm/yr, but there are also three discontinuities leading to shorter ranges that likely result from monument instability at the time of strong earthquake-induced shaking. The red lines indicate the slope that would be expected if the C2-P5 baseline straddled a fault that creeped continuously at the plate-motion rate (14 cm/yr). If the C2-P5 baseline does cross the plate boundary, the lack of a significant ∼10 cm/yr slope in these data indicates that the fault is predominately locked in this region.

variation results from the overall ~3 cm/yr increase in range observed for this baseline. Thus, there is no clear decrease in precision with increasing baseline length for 300–750 m baselines. Moreover, the 512 bit code used in the acoustic ranging provides some of the most precise travel time measurements to date, at least in deep water settings like fault valleys where the sound speed corrections are relatively straightforward.

[13] We do not draw any strong geophysical conclusions from the measurements presented in this section because our instruments were not installed in a robust manner, such as on concrete piers poured by an ROV for this purpose. Many (all?) of the offsets are likely due to instrument instability rather than fault motion. However, the ~3 cm/yr trend of increasing ranges observed on the C2-P5 baseline is not immediately dismissable as an artifact of monument instability. This baseline crossed the fault valley where it is most sharply defined, and it is likely that this baseline spans the plate boundary. Owing to its left-lateral motion, if this fault were continuously creeping at the plate-motion rate (~14 cm/yr), we would expect this baseline to get longer at a rate of ~10 cm/yr. Figure 11 shows the large difference between the signal expected for a fully creeping fault and the slight trend to increasing baseline length with time that we observe. If the plate boundary does pass through the C2-P5 baseline, then our measurements would be consistent with close to full locking in this region. While our result is not conclusive due to benchmark instability and the uncertainty in the location of the fault trace, it is in agreement with studies of large, M6.0, repeating earthquakes that suggest nearly full interseismic locking on this portion of the discovery transform fault [*Wolfson et al*., 2011].

## 4. Conclusions

[14] Direct-path acoustic ranging is an important seafloor geodetic technique for continuously monitoring seafloor volcanoes and plate boundary faults. The primary limitations on its accuracy result from the need to correct for sound-speed variations, the design of the acoustic signal, and benchmark stability. We have demonstrated that the first two can be readily overcome at the 1 mm level for monitoring oceanic transform faults. The use of benchmarks carefully emplaced by submersible or ROV would allow acoustic ranging to detect both seismic and aseismic fault slip on transform faults with very high precision. While one baseline is not enough to be conclusive, our results are consistent with a high degree of interseismic locking on the Discovery transform fault in the region of our array.

## Acknowledgments

[15] We thank the crews of the R/V Thomas G. Thompson and the R/V Atlantis for their help with instrument deployment and recovery. Don Forsyth provided multibeam bathymetry data prior to the deployment cruise. We thank R. Pickle for shipboard processing of the EM300 bathymetry data acquired from the R/V Thomas G. Thompson, and M. Wolfson for providing the final processed bathymetry map shown in Figure 1. We thank two anonymous reviewers for comments that improved the manuscript. This research was funded by the National Science Foundation OCE division under award 0351143.

## References

Bird, P., Y. Y. Kagan, and D. D. Jackson (2002), Plate tectonics and earthquake potential of spreading ridges and oceanic transform faults, in *Plate Boundary Zones*, edited by S. Stein and J. T. Freymueller, pp. 203–218, AGU, Washington, D. C.

Blum, J. A., C. D. Chadwell, N. Driscoll, and M. A. Zumberge (2010), Assessing slope stability in the Santa Barbara Basin, California, using seafloor geodesy and CHIRP seismic data, *Geophys. Res. Lett.*, *37*, L13308, doi:10.1029/2010GL043293.

Boettcher, M. S., and T. H. Jordan (2004), Earthquake scaling relations for mid-ocean ridge transform faults, *J. Geophys. Res.*, *109*, B12302, doi:10.1029/2004JB003110.

Boettcher, M. S., and J. J. McGuire (2009), Scaling relations for seismic cycles on mid-ocean ridge transform faults, *Geophys. Res. Lett.*, *36*, L21301, doi:10.1029/2009GL040115.

Chadwell, C. D., and F. N. Spiess (2008), Plate motion at the ridge-transform boundary of the south Cleft segment of the Juan de Fuca Ridge from GPS-Acoustic data, *J. Geophys. Res.*, *113*, B04415, doi:10.1029/2007JB004936.

Chadwell, C. D., J. A. Hildebrand, F. N. Spiess, J. L. Morton, W. R. Normark, and C. A. Reiss (1999), No spreading across the southern Juan de Fuca Ridge axial cleft during 1994–1996, *Geophys. Res. Lett.*, *26*(16), 2525–2528.

Chadwick, W. W., and M. Stapp (2002), A deep-sea observatory experiment using acoustic extensometers: Precise horizontal distance measurements across a mid-ocean ridge, *IEEE J. Ocean. Eng.*, *27*(2), 193–201.

Chadwick, W. W., R. W. Embley, H. B. Milburn, C. Meinig, and M. Stapp (1999), Evidence for deformation associated with the 1998 eruption of Axial Volcano, Juan de Fuca Ridge, from acoustic extensometer measurements, *Geophys. Res. Lett.*, *26*(23), 3441–3444.

Cowie, P. A., C. H. Scholz, M. Edwards, and A. Malinverno (1993), Fault strain and seismic coupling on mid-ocean ridges, *J. Geophys. Res.*, *98*(B10), 17,911–17,920.

Gagnon, K., C. D. Chadwell, and E. Norabuena (2005), Measuring the onset of locking in the Peru-Chile trench with GPS and acoustic measurements, *Nature*, *434*, 205–208.

McGuire, J. J. (2008), Seismic cycles and earthquake predictability on east pacific rise transform faults, *Bull. Seismol. Soc. Am.*, *98*(3), 1067–1084.

McGuire, J. J., M. S. Boettcher, and T. H. Jordan (2005), Foreshock sequences and short-term earthquake predictability on East Pacific Rise transform faults, *Nature*, *434*(7032), 457–461.

McGuire, J. J., J. A. Collins, P. Gouedard, E. Roland, D. Lizarralde, M. S. Boettcher, M. D. Behn, and R. D. van der Hilst (2012), Capturing the end of a seismic cycle on the gofar transform fault, *East Pacific Rise, Nat. Geosci.*, *5*(5), 336–341.

Osada, Y., M. Kido, H. Fujimoto, and Y. Kaneda (2008), Development of a seafloor acoustic ranging system toward the seafloor cable network system, *Ocean Eng.*, *35*, 1401–1405.

Osada, Y., M. Kido, and H. Fujimoto (2012), A long-term seafloor experiment using an acoustic ranging system: Precise horizontal distance measurements for detection of seafloor crustal deformation, *Ocean Eng.*, *51*, 28–33.

Pickle, R. C., D. W. Forsyth, N. Harmon, A. N. Nagle, and A. Saal (2009), Thermo-mechanical control of axial topography of intra-transform spreading centers, *Earth Planet. Sci. Lett.*, *284*(3–4), 343–351.

Roland, E., and J. J. McGuire (2009), Earthquake swarms on transform faults, *Geophys. J. Int.*, *178*(3), 1677–1690.

Spiess, F. N., C. D. Chadwell, J. A. Hildebrand, L. E. Young, G. H. Purcell Jr., and H. Dragert (1998), Precise GPS/acoustic positioning of seafloor reference points for tectonic studies, *Phys. Earth Planet. Inter.*, *108*, 101–112.

Wei, M., Y. Kaneko, Y. Liu, and J. J. McGuire (2013), Episodic fault creep events in California controlled by shallow frictional heterogeneity, *Nat. Geosci.*, *6*, 566–570.

Wolfson, M., M. S. Boettcher, J. J. McGuire, and J. Collins (2011), Absolute locations of repeating mw 5.5–6.0 earthquakes on the discovery transform fault, EPR, Abstract T23C-2419 presented at 2011 Fall Meeting, AGU, San Francisco, Calif., 5–9 Dec.